AIP | Applied Physics Letters

Fabrication of 10 nm diameter hydrocarbon nanopores

Aleksandra Radenovic, Eliane Trepagnier, Roseann Csencsits, Kenneth H. Downing, and Jan Liphardt

Citation: Applied Physics Letters **93**, 183101 (2008); doi: 10.1063/1.3012376

View online: http://dx.doi.org/10.1063/1.3012376

View Table of Contents: http://scitation.aip.org/content/aip/journal/apl/93/18?ver=pdfcov

Published by the AIP Publishing

Fabrication of 10 nm diameter hydrocarbon nanopores

Aleksandra Radenovic,[1,a)] Eliane Trepagnier,[1,2,b)] Roseann Csencsits,[3] Kenneth H. Downing,[3] and Jan Liphardt[1,2,3]
[1]*Department of Physics, University of California–Berkeley, California 94720, USA*
[2]*Biophysics Graduate Group, University of California–Berkeley, California 94720, USA*
[3]*Physical Biosciences Division, Lawrence Berkeley National Laboratory, Berkeley, California 94720, USA*

(Received 8 June 2008; accepted 7 October 2008; published online 3 November 2008)

The addition of carbon to samples, during transmission electron microscope imaging, presents a barrier to accurate analysis; the controlled deposition of hydrocarbons by a focused electron beam can be a useful technique for local nanometer-scale sculpting of material. Here we use hydrocarbon deposition to form nanopores from larger focused ion beam holes in silicon nitride membranes. Using this method, we close 100–200 nm diameter holes to diameters of 10 nm and below, with deposition rates of 0.6 nm/min. *I-V* characteristics of electrolytic flow through these nanopores agree quantitatively with a one dimensional model at all examined salt concentrations. © *2008 American Institute of Physics*. [DOI: 10.1063/1.3012376]

Synthetic nanopores have gained considerable interest for applications ranging from single-molecule DNA sequencing[1] to studies of DNA-protein interactions,[2] RNA folding kinetics,[3,4] and single-molecule force measurements.[5,6] Solid-state nanopores have several desirable properties, including tunability of surface chemistry and size, compatibility with electronic sensing systems, improved pore lifetime, mechanical stability, and sizes comparable to the cross section of biomolecules.

While nanopores are a promising technology for single-molecule measurements, they remain difficult to create, often requiring very expensive and specialized instruments. A variety of approaches have been used to prepare synthetic nanopores. One such method is ion beam sculpting, where relatively large focused ion beam (FIB) holes are closed down to 2–10 nm using a defocused argon ion beam.[7] Other methods include electron beam-induced pore closing,[8] electron beam stimulated decomposition and sputtering,[9,10] film embedding of carbon nanotubes,[11] soft lithography,[12] and chemical etching.[13,14]

Once created, nanopores must be measured. The scale of these pores (2–10 nm in diameter) requires extremely high-resolution measurement techniques and is typically done by transmission electron microscope (TEM). TEM measurement of pore size contributes substantially to fabrication times. An advantage of TEM-based fabrication techniques[8,10,15] is that creation and measurement steps can be combined, greatly shortening overall processing time. So far all TEM-based fabrication techniques require a field emission gun (FEG) to achieve the necessary electron density. The most straightforward of these, drilling holes in thin silicon oxide (SiO_2) or silicon nitride (Si_3N_4) membranes, requires a beam intensity of 10^8e nm^{-2}.[9] In another TEM-based scheme, an electron beam of intensity 10^7e nm^{-2} is used to locally melt the membrane surrounding an ~20 nm pore, leading to nanopore contraction driven by surface energy minimization.

While small nanopores are difficult to create, large pores (100–200 nm diameter) are easy to fabricate using FIB drilling. In this paper, we describe a method to make nanopores from larger FIB holes with starting diameters of 50–200 nm, using a standard (non-FEG) TEM. Because this method does not require specialized equipment it is available to anyone with access to a standard TEM.

Our method is based on the familiar phenomenon of carbon contamination. Carbon contamination in TEM is a well known phenomenon. During this process, hydrocarbons adsorbed on sample surfaces are polymerized and immobilized by a high-energy electron beam. Hydrocarbons present on TEM samples migrate into the electron beam, where they are cross linked and immobilized. Carbon contamination scatters incident high-energy electrons,[16] can obscure measurement, and is generally undesirable in TEM work. However, buildup of carbonaceous material is slow and localized to the electron beam and thus a useful tool for nanometer-scale sculpting. Hydrocarbon contamination lithography that was first proposed in 1976 by Broers *et al.*[17] has been recently used as a nanofabrication tool creating nanowires,[18] nanostructures,[19,20] and sharp scanning probe microscopy (SPM) tips.[21,22]

A buildup of a low-*Z* hydrocarbon layer during electron beam exposure in scanning electron microscope has been previously used to fabricate nanometer-scale holes in nitride membranes.[23] Here, we use hydrocarbon contamination lithography to selectively and controllably add material for nanopore closure in TEM. There are two advantages over method proposed in Ref. 23; our method posses higher accuracy and it allows monitoring of nanopore formation in real time while pores are ready for use in consequent experiments.

Our nanopores are fabricated in SPI silicon nitride TEM grids, or in silicon chips diced from custom wafers. These wafers were made as follows. First, low-pressure chemical vapor deposition is used to grow a 200 nm thick Si_3N_4 film on the surface of a Si wafer. (We have chosen Si_3N_4 over SiO_2 due to its superior mechanical properties.[10]) We exposed the silicon nitride membrane in 50×50 μm^2 windows using photolithography and standard KOH etching.

In the center of each window, we thinned the silicon nitride membrane to ~20 nm in a 1×1 μm^2 circular area

[a)]Author to whom correspondence should be addressed. Present address: LBEN, IBI2, Ecole Polytech Fed Lausanne, CH-1015 Lausanne, Switzerland. Electronic mail: aleksandra.radenovic@epfl.ch.
[b)]Present address: Department of Biochemistry, Stanford University, Stanford, CA 94305.

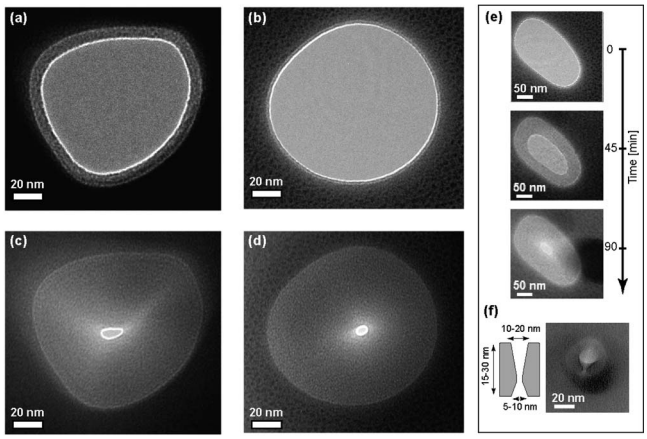

FIG. 1. [(a)–(d)] Transmission electron microscopy (JEOL 4000) images of two FIB holes that have been closed from a starting diameter of 100–200 nm down to 10–20 nm. Before (top row) and after (bottom row) carbon deposition. FIB holes of 100–200 nm in diameter were imaged and exposed to a high-energy (400 keV) beam for carbon deposition. Panel (e) shows a time series of the carbon deposition process. (f) Cross-sectional schematic of fabricated nanopores and TEM micrograph of 30° tilted nanopore.

using a FIB (FEI Strata 235 dual beam). Milling time and ion beam current settings were optimized on a sacrificial sample in each FIB run. Finally, in the center of that region we drill a pore of 50–150 nm in diameter. To drill holes in this thinned area and to achieve a sufficient small beam diameter, the experiments were carried out with the ion acceleration voltage and current set to 30 keV Ga+beam with an intensity of 10 pA in spot and a diameter of 10 nm (full width at half maximum).

The Ga^+ ion beam allows ion beam assisted drilling, thinning, and deposition, while electron beam allows *in situ* characterization such as scanning electron microscopy and energy dispersive x-ray spectroscopy. Hydrocarbon deposition and imaging of the nanopores were carried out in a JEOL 4000, equipped with a $2K \times 2K$ Gatan charge-coupled device camera and Gatan TV camera. As the initial FIB holes shown on Figs. 1(a) and 1(b) are exposed to the focused electron beam (at room temperature and 1.5×10^{-7} torr) the carbon contamination slowly builds up. By moving the highly focused e-beam we could create pores with diameters of 10 nm or less, as shown on Figs. 1(c) and 1(d). Figure 1(e) displays intermediate steps in the pore closing process. These real-time measurements of pore diameter give nanometer control over pore closing. The observed rate of carbon deposition was proportional to the sample thickness. Additional factors controlling the amount of carbon contamination include sample preparation steps, the adhesiveness of the sample to hydrocarbons, the vacuum level of the microscope, sample temperature, hydrocarbon contamination in the microscope, outgassing from o rings and stage lubricant, contamination due to back streaming pump oil, and electron probe current density.[24] To further examine nanopore shape, we took TEM micrographs with the sample tilted at 30° [Fig. 1(f)]. TEM micrographs suggest an "hour-glass-shaped" nanopore. Initial thickness of thinned SiN is 15–30 nm which determines the nanopore channel length. The channel has an "hour-glass-like" shape, with a diameter ranging from 5 to 10 nm in the narrowest section and 10–20 nm at each end, as shown on the schematic in Fig. 1(f).

Carbon contamination is a combination of several effects. Hydrocarbon molecules are adsorbed onto the sample surface either during sample preparation or inside the microscope.[16] Molecular adsorption is governed by the relation $f \propto \sqrt{(m/T)}p$, where f is the flux of molecules adsorbed to the surface, m the mass of hydrocarbon molecules, p the partial pressure of the hydrocarbon, and T the absolute temperature.[16] Once adsorbed, these molecules diffuse across the surface due to thermal, electrical, or chemical gradients[16] (all of which are produced by electron beams). Primary and secondary electrons formed from beam-sample interactions near exposed areas excite and rupture common –CH, –COOH, –CNH2, and other bonds, resulting in the release of nonvolatile molecules and the formation of carbon double bonds. Finally, polymerization and immobilization of the hydrocarbons build up on the surface.[25]

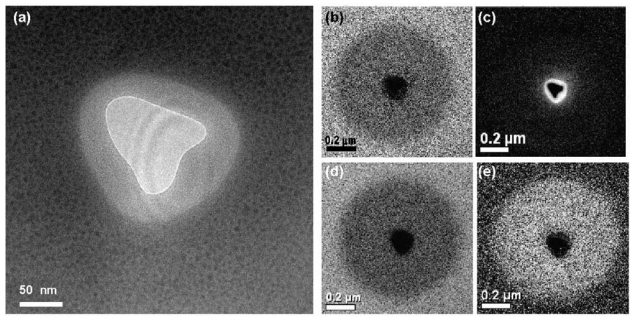

FIG. 2. (Color online) (a) TEM image of carbon nanopore. (b) Elemental nitrogen, (c) carbon, (d) silicon, and (e) gallium EELS maps of the pore. Pores are fabricated in silicon nitride membranes. The membrane is thinned using a focused beam of gallium ions, some of which are incorporated into the membrane, as seen in panel (e). Finally, the pore is sculpted in a TEM. The material added is clearly carbonaceous, as can be seen in panel (c).

The chemical gradient produced by this carbonaceous area is filled in by diffusion of hydrocarbons from outside the irradiated area. Diffusion is further enhanced by sample heating (due to the interaction of the electron beam with the sample) and sample charging resulting from emission of secondary electrons.[16] Electron-energy loss spectroscopy (EELS) experiments and elemental mapping were performed to determine the chemical composition of the fabricated nanopores. The results of the EELS measurements are shown in Fig. 2. Panel (a) shows a 100KX TEM image of a nanopore; panels (b)–(e) show the four corresponding maps of nitrogen, carbon, silicon, and gallium. These elemental maps show clearly that the material forming the nanopore is carbonaceous [Fig. 2(b)]. In addition, the starting material, silicon nitride, along with the gallium ions incorporated during substrate thinning are present on 1×1 μm^2 center area but largely absent from the inner pore. Energy filtered elemental maps were acquired in the JEOL 2010 TEM equipped with a Gatan Tridiem imaging filter, with 200 kV electrons operating in conventional TEM imaging mode. The three-window method (two pre-edge and one postedge) was used to model and remove background to give optimum edge signal for each element. The windows used for the N, C, Si, and Ga maps were 30, 20, 50, and 50 eV, respectively, with acquisition times of 10, 10, 30, and 30 s. To demonstrate the functionality of the fabricated nanopores we performed electrophoretic ion transport measurements. A silicon chip with a single nanopore was fixed horizontally in a poly(dimethylsiloxane) chamber located in a Faraday cage. The chamber design is compatible with our optical system described elsewhere.[6] Both fluid chambers were connected to the ex-

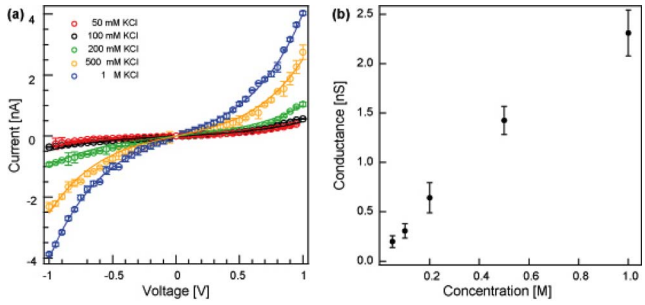

FIG. 3. (Color online) (a) *I-V* curves for a 10 nm diameter carbon nanopore. (b) Conductance as a function of KCl concentration at *p*H 7.5 for same carbon nanopore.

ternal measuring circuit using Pt electrodes. The electrode in the top fluid chamber was connected to the head stage of an Axopatch 200B amplifier operating in the voltage clamp mode while the bottom electrode was grounded. We measured dc through a single nanopore as a function of the applied potential. We took a series of current-voltage measurements at KCl concentrations ranging from $0.05-1M$ and *p*H 7.5. The current-voltage characteristics of these nanopores [Fig. 3] at all salt concentration were highly nonlinear. The nonlinearity of ionic current in nanofluidic systems is known to result from asymmetric nanopore shape and/or charge distribution. Form EELS measurements we know that our nanopores are made from hydrocarbons suggesting that our pores might be highly hydrophobic and negatively charged and in that sense very similar to biological pores[26] and channels.[27] Recent theoretical[28] and experimental studies[29] suggest an existence of surface charge which depends on the pore material.

At neutral and basic *p*H, the carboxylate groups in hydrocarbon nanopores are deprotonated, resulting in an excess negative surface charge and finally an internal electrostatic potential. It has been observed[14] and calculated[28] that pore shape dictates the profile of internal electrostatic potential. For example, in conical pores this profile looks like an asymmetric "ratchet" tooth[14] and results in an asymmetric diode-like current-voltage characteristic. In contrast, our current-voltage characteristics, while nonlinear, are symmetric at all salt concentrations suggesting cylindrical shape of fabricated nanopores.

A model of electrolyte transport properties developed for asymmetric (nonconical) charged pores[28] also gives satisfactory fits of our data [Fig. 3(a)], implying that nonlinear *I-V* characteristics are likely due to the existence of internal electrostatic potential. The model, described in detail elsewhere,[28] is based on the reduction in the three-dimensional Smoluchowski equation[30] into one-dimensional equation of Fick–Jackobs type. We have also calculated experimental values for the conductance as an average over the voltage range $(-1 \ V \leq V \geq 1)$ at *p*H 7.5. The ionic conductance inside the nanopore linearly increased with the electrolyte concentration [Fig. 3(b)].

To conclude, we have shown that controlled deposition of hydrocarbons can be used to make nanopores, using standard widely available FIB and TEM technology. Our technique provides three main advantages over current nanopore fabrication methods. First, the slow deposition rates of carbon (0.6 nm/min) permit a high degree of control over nanopore size and location. Second, it does not require special equipment. Finally, because fabrication is performed in a TEM, this method permits simultaneous size measurement of the nanopores. We show that the resulting pores exhibit interesting nonlinear *I-V* characteristics. The fabricated nanopores should be useful as components of nanofluidic sieving and molecular sensing devices.

We thank the National Center for Electron Microscopy (NCEM) at LBL for providing access to TEM and FIB. We thank the anonymous referee for valuable suggestions. For financial support, we thank the UC Biotechnology Research and Education Program (E.T.) and the Swiss National Science Foundation (A.R.). This work was supported in part by the University of California–Berkeley, the Hellman Faculty Fund, the Sloan and Searle Foundations (J.L.), the DOE Office of Science, Energy Biosciences Program KC0304 under Contract No. DE-AC03-76SF00098, and the U.S. Department of Energy under Contract No. DE-AC02-05CH11231. A.R. and E.T. contributed equally to this work.

[1] H. Yan and B. Q. Xu, Small **2**, 310 (2006).
[2] B. Hornblower, A. Coombs, R. D. Whitaker, A. Kolomeisky, S. J. Picone, A. Meller, and M. Akeson, Nat. Methods **4**, 315 (2007).
[3] R. Bundschuh and T. Hwa, Phys. Rev. Lett. **83**, 1479 (1999).
[4] U. Gerland, R. Bundschuh, and T. Hwa, Biophys. J. **81**, 1324 (2001).
[5] U. F. Keyser, B. N. Koeleman, S. Van Dorp, D. Krapf, R. M. M. Smeets, S. G. Lemay, and N. H. Dekker, Nat. Phys. **2**, 473 (2006).
[6] E. H. Trepagnier, A. Radenovic, D. Sivak, P. Geissler, and J. Liphardt, Nano Lett. **7**, 2824 (2007).
[7] J. Li, D. Stein, C. McMullan, D. Branton, M. J. Aziz, and J. A. Golovchenko, Nature (London) **412**, 166 (2001).
[8] A. J. Storm, J. H. Chen, X. S. Ling, H. W. Zandbergen, and C. Dekker, Nature Mater. **2**, 537 (2003).
[9] C. Ho, R. Qiao, J. B. Heng, A. Chatterjee, R. J. Timp, N. R. Aluru, and G. Timp, Proc. Natl. Acad. Sci. U.S.A. **102**, 10445 (2005).
[10] M. Y. Wu, D. Krapf, M. Zandbergen, H. Zandbergen, and P. E. Batson, Appl. Phys. Lett. **87**, 113106 (2005).
[11] R. R. Henriquez, T. Ito, L. Sun, and R. M. Crooks, Analyst (Cambridge, U.K.) **129**, 478 (2004).
[12] O. A. Saleh and L. L. Sohn, Nano Lett. **3**, 37 (2003).
[13] S. R. Park, H. B. Peng, and X. S. S. Ling, Small **3**, 116 (2007).
[14] Z. Siwy and A. Fulinski, Phys. Rev. Lett. **89**, 198103 (2002).
[15] M. Kim, M. Wanunu, D. C. Bell, and A. Meller, Adv. Mater. (Weinheim, Ger.) **18**, 3149 (2006).
[16] J. J. Hren, J. I. Goldstein, and D. C. Joy, *Introduction for Analytical Electron Microscopy* (Plenum, New York, 1979).
[17] A. N. Broers, W. W. Molzen, J. J. Cuomo, and N. D. Wittels, Appl. Phys. Lett. **29**, 596 (1976).
[18] C. H. Jin, J. Y. Wang, Q. Chen, and L. M. Peng, J. Phys. Chem. B **110**, 5423 (2006).
[19] H. Konuma, Mikrochim. Acta **2**, 99 (1983).
[20] K. Ueda and M. Yoshimura, Thin Solid Films **464**, 331 (2004).
[21] S. D. Johnson, D. G. Hasko, K. B. K. Teo, W. I. Milne, and H. Ahmed, Microelectron. Eng. **61**, 665 (2002).
[22] B. Hubner, H. W. P. Koops, H. Pagnia, N. Sotnik, J. Urban, and M. Weber, Ultramicroscopy **42**, 1519 (1992).
[23] T. Schenkel, V. Radmilovic, E. A. Stach, S. J. Park, and A. Persaud, J. Vac. Sci. Technol. B **21**, 2720 (2003).
[24] T. C. Isabell, P. E. Fischione, C. O. O'Keefe, M. U. Guruz, and V. P. Dravid, Microscopy and Analysis **5**, 126 (1999).
[25] L. Reimer, *Scanning Electron Microscopy* (Springer, Berlin, 1985).
[26] S. A. Spronk, D. E. Elmore, and D. A. Dougherty, Biophys. J. **90**, 3555 (2006).
[27] T. Okazaki, M. Sakoh, Y. Nagaoka, and K. Asami, Biophys. J. **85**, 267 (2003).
[28] A. Fulinski, I. Kosinska, and Z. Siwy, New J. Phys. **7**, 132 (2005).
[29] Z. Siwy, P. Apel, D. Baur, D. D. Dobrev, Y. E. Korchev, R. Neumann, R. Spohr, C. Trautmann, and K. O. Voss, Surf. Sci. **532**, 1061 (2003).
[30] M. von Smoluchowski, Ann. Phys. **21**, 756 (1906).